_____

# Big Data Classification of Ultrasound Doppler Scan Images Using a Decision Tree Classifier Based on Maximally Stable Region Feature Points

[a] **S. Sandhya Kumari**
[a] Research Scholar, Dept. of Computer Science,
SPMVV,Tirupati,India
sridharamsandhya@gmail.com

[b] **K. Sandhya Rani**
[b] Professor, Dept. of Computer Science,
SPMVV, Tirupati, India
sandhyarani.kasireddy@gmail.com

**Abstract**— The classification of ultrasound scan images is important in monitoring the development of prenatal and maternal structures. This paper proposes a big data classification system for ultrasound Doppler scan images that combines the residual of maximally stable extreme regions and speeded up robust features (SURF) with a decision tree classifier. The algorithm first preprocesses the ultrasound scan images before detecting the maximally stable extremal regions (MSER). A few essential regions are chosen from the MSER regions, along with the residual region that provides the best Region of Interest (ROI). SURF features points that best represent the region are detected using the gradient of the estimated cumulative region of interest. To extract the feature from the pixels that surround the SURF feature points, the Triangular Vertex Transform (TVT) transform is used. A decision tree classifier is used to train the extracted TVT features. The proposed ultrasound scan image classification system is validated using performance parameters such as accuracy, specificity, precision, sensitivity, and F1 score. For validation, a large dataset of 12,400 scan images collected from 1792 patients is used. The proposed method has an F1score of 94.12%, sensitivity, specificity, precision, and accuracy of 93.57%, 93.57%, and 97.96%, respectively. The evaluation results show that the proposed algorithm for classifying Doppler scan images is better than other algorithms that have been used in the past.

**Keywords**- Maximally stable extremal regions, Ultrasound scan images, Triangular vertex transform, Speeded up robust features, and Decision tree classifier.

## 1. INTRODUCTION

Doppler ultrasound scan is a non-invasive less expensive imaging procedure that is used to monitor the internal maternal structure and growth of fetal organs during the gestation period. This monitoring helps to estimate the Doppler blood flow, abnormalities in the fetal organs, fetal weight, and internal structure of the mother. The monitoring of the internal structure of the mother helps to predict the complexity during pregnancy or delivery. During the gestation period, the movement of the fetus will create degradation in image quality of Magnetic Resonance Image (MRI) scanning, and it creates difficulty in identifying the fetal organs or mother's internal structures. Ultrasound Doppler scan imaging procedure is more robust to fetal movement than in MRI imaging procedure; hence the degradation will be minimum. In Doppler scan images, the shape, texture, and morphology volume of fetal organs are accessed to estimate the pregnancy complication and fetal health. Intra-observer variability and inter-observer variability can lead to wrong ultrasound Doppler scan image classification results. Also, it is difficult for the physician to manually classify the images since more than 20 images are generated in a single ultrasound examination during the second trimester. This manual classification also creates variation in the fetal position and gestational age estimation. Even though the ultrasound Doppler scanning procedure has the challenges like the low field of view, low contrast, beam attenuation created by adipose tissue, it has a valuable advantage such as low cost and is less harmful to both fetus and mother.

Deep learning and machine learning algorithms play a major role in biomedical image classification [1]. Machine learning algorithms are highly preferred where feature extraction is possible from the ROI. This feature extraction technique aims to extract the feature, shape, and color features from the ROI. The feature extraction methods include algorithms like Histogram of Oriented Gradient (HOG) [2], Local Directional Pattern (LDP) [4],Local Binary Pattern (LBP) [3], etc. Once the feature extraction process completes, the features that are extracted from the training images are trained using machine learning algorithms like support vector machine [5], multilayer perceptron [6], etc. Before extracting the features pre-processing and segmentation are performed. The pre-

_____

processing aims to highlight the features/region of interest where the segmentation aims to detect the ROI. The pre-processing includes scaling, filtering that highlights the region of interest. The segmentation algorithm includes the schemes such as thresholding [7], morphological processing such as dilation, and erosion [8], edge-based, and region-based segmentation algorithms. Deep learning algorithms are preferred over machine learning algorithms where it is difficult to identify the ROI or in extracting the features from the ROI. Convolutional Neural Network (CNN)plays a crucial role in deep learning whichis used in different applications such as MRI imaging [9], fundus image [10], dermatology [11], Optical Coherence Tomography (OCT) [12], radiology [13], etc. The CNN will estimate the complex patterns when the network is trained.

Different convolutional and pooling structures are used by the author Li et al. [14], where the amniotic fluid and the fetal tissues are classified. This approach provides an accuracy of 67% in detecting the fetal body. The normal and abnormal brain scan images are classified by Attallah et al. [15] where the authors used random forest and Naïve Bayes classifiers along with kNN (k-nearest neighbour)and diagonal quadratic discriminant analysis. Local and global features [16] are also extracted to classify the 14 fetal structures. Different networks such as GoogleNet, CNN, and AlexNex are used by the authors Selvanthi et al. [17] that can detect the abnormality in which the classifier AlexNet provides an accuracy of 90.43%. From the fetal ultrasound scan image, congenital heart disease can be detected where the explainable residual learning scheme [18] is used by the authors Sibo et al. that provide an accuracy of 93%. The support vector machines along with statistical features are used by the authors Sushma et al. [19] that estimate the patterns. This approach extracts the fetus's cardiac anatomical structure using the convolutional neural network and the discriminative features. The authors Maraci et al.

[20] used conditional random field (CRF) for detecting the heartbeat from the video frames. The authors Ryou et al. [21] classified different parts of the fetus namely fetal head, fetal body, and other regions using CNN. This approach is semi-automatic which also requires additional clinical information like biometry plane position to detect the head/body. The authors' Li et al. [22] detected the fetal brain using an iterative approach CNN with multiple passes.

However, extracting the features from the regions that highly correlate with the region of interest can further progressthe performance of the classification algorithm. The contributions of the work are as follows,

The algorithm initially extracts the maximally stable region that includes the few regions of interest and background region.

The algorithm also proposes a region selection that eliminates the regions that do not contain the feature information.

The residual region and a few regions selected by the region selection process are used to extract the essential features. SURF feature points are detected using the gradient obtained on the estimated region of interest.

The paper also proposes a triangular vertex transform-based feature extraction algorithm that uses neighboring pixels around the SURF feature points.The extracted features are trained using a decision tree-based classifier.

Finally, the performance validation was done using the performance parameters namely precision, specificity, F1 Score, accuracy, and sensitivity.

The forthcoming section of the paper is constructed as follows, section 2 depicts the proposed ultrasound doppler scan image classification system, section 3 shows the experimental results and analysis of the proposed system and finally, section 4 provides the conclusion of the work.

_____

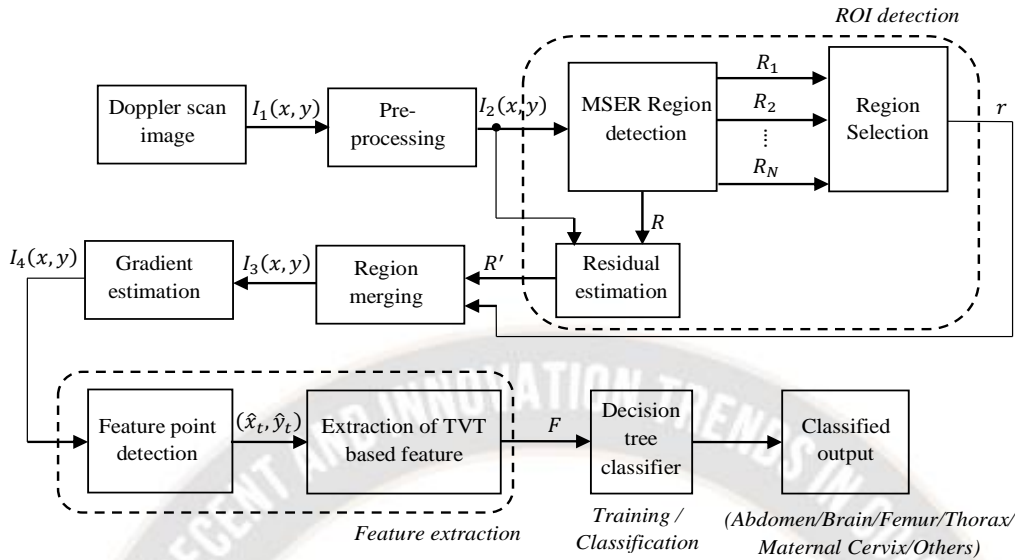## 2. PROPOSED FETAL SCAN IMAGE CLASSIFICATION



**Fig 1**: Block diagram representation of the proposed ultrasound scans image classification

The proposed ultrasound scan image classification includes processes such as preprocessing, ROI detection, Feature extraction, and decision tree classifier as provided in the block diagram shown in Fig 1.

### 2.1 Preprocessing

The ultrasound doppler scan image $I_1(x, y)$ be initially filtered using a median filter and resized to a uniform size. Let the Doppler scan image after preprocessing be $I_2(x, y)$ having a size of $U \times V$.

### 2.2 ROI detection

The ROI detection includes the estimation of $N$ number of maximally stable extremal regions which is detected using the MSER detection algorithm [23].

#### (a) Maximally stable extremal region (MSER)

The MSER algorithm extracts the region of interest that contains connected components which are estimated by the stability factor

$$\varepsilon(\delta) = \frac{Area(\rho_\delta)}{\frac{d}{d\delta}(Area(\rho_\delta))} \quad (1)$$

Where, $\rho_\delta$ represents the connected component (region), the connected component $\rho_\delta$ is stable, for a slight change of threshold if there existsa slight change in the area. If $\varepsilon(\delta)$ has a local maximum with threshold $\delta$, then the connected component is said to be maximally stable. For the threshold $\delta$, the growth rate function in the region $\rho$ is expressed as,

$$\gamma(\delta) = \frac{\frac{d}{d\delta}(Area(\rho_\delta))}{Area(\rho_\delta)}$$

$$(2)$$

The MSER detection algorithm returns $N$ number of maximally stable regions represented as $R_n = \{R_1, R_2, R_3 \dots \dots R_N\}$.

#### (b) Region selection and region merging

The region covered by the MSER algorithm is given

$$R = R_1 \cup R_2 \cup R_3 \dots \dots \cup R_N = \cup_{n=1}^{N} R_n$$

$$(3)$$

The region that was not covered by the MSER algorithm gives the residual region given by

$$R' = I_R - R \quad (4)$$

Here $I_R$ is the complete region of the image $I_2(x, y)$, where ($\cup$) and (-) are the set union and difference operator respectively. In region merging, the residual region $R'$ and few MSER regions $r$ are merged to construct the region $\hat{r}$, such that the merged region is expressed as

$$\hat{r} = R' \cup r \quad (5)$$

The region $r$ is selected by the region selection process. The selection was done based on the correlation function. Let $A_n = \{A_1, A_2 \dots \dots A_N\}$ be the area of the regions $R_1 = \{R_1, R_2 \dots \dots R_N\}$. The normalized area is estimated from the area of the regions as

$$\hat{A}_n = \frac{A_n}{U \times V} \quad (6)$$

where $\hat{A}_n = \{\hat{A}_1, \hat{A}_2 \dots \dots \hat{A}_N\}$. The correlation of the pixels between the residual region $R'$ and $R_n$ is represented as $\tau_n = \{\tau_1, \tau_2 \dots \dots \tau_n\}$.A region from $R_n$ is

selected, if the product of correlation of the respective region $\tau_n$ and the cumulative normalized area of other regions $\hat{a}_m$ is greater than the product of the cumulative correlation of the other region and the normalized area of the region $R_n$ mathematically expressed as

$$\tau_n \hat{a}_m > \hat{\tau}_m \hat{A}_n \qquad (7)$$

where $\hat{\tau}_n$ is the correlation between the $\bigcup_{j \neq n} R_j$ and the residual region $R'$ and the area $\hat{a}_m$ can be estimated by

$$\hat{a}_m = \sum_{j \neq n} \hat{A}_n \qquad (8)$$

The regions that satisfy the condition $\tau_n \hat{a}_m > \hat{\tau}_m \hat{A}_n$ is also selected for extracting the features along with the residual region. Let the regions that satisfy the above condition be $r_k = \{r_1, r_2 \ldots \ldots r_K\}$, where $K$ be the number of MSER regions that are chosen by the region selection process for feature extraction along with the residual region. Thus the region selected is given by

$$r = \bigcup_{k=1}^{K} r_k. \qquad (9)$$

The selected regions $r$ and the residual regions $R'$ are merged using the relation $\hat{r} = R' \cup r$ to obtain the complete region $\hat{r}$ for extraction of features and the remaining regions are excluded from feature extraction and the pixels that correspond to the other regions are made zero. Let $I_3(x, y)$ be the pixels that correspond to the region $\hat{r}$. The gradient [24] is then estimated on region $\hat{r}$ having the intensities of the pixels $I_3(x, y)$. Let $I_4(x, y)$ be the magnitude of the gradient obtained on the image $I_3(x, y)$. The gradient highlights the features present in the ROI for extracting the features.

## 2.3. Feature extraction

Theextraction of feature is done in two steps namely detection of SURF feature points and extraction of TVT features in the neighborhood of SURF feature points. From $I_4(x, y)$ the feature points are estimated using the SURF algorithm.

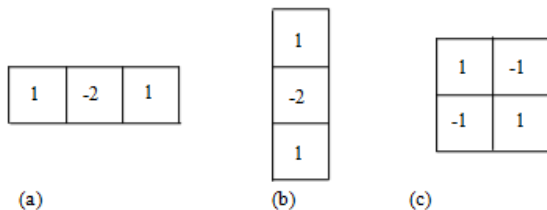    *(a) **SURF feature point detection (Speeded up robust features points)***



**Fig 2:**Second order derivative in (a)$C_{pp}$ (b)$C_{qq}$ (c) $C_{pq}$ .

SURF features [25] are invariant to in-plane rotation and scaling.The SURF features are extracted in two steps. Initially, the interest point is detected and then the descriptor is extracted from the point of interest. The SURF

detector estimates blob-like structures in the Doppler image. In the Doppler scan image, the blob-like structures are found in the region of interest. The SURF algorithm constructs a box filter that appears like a pyramid scale space. The determinant of Hessian is used to detect the interest point. Let $G = (p, q)$ represent a point in an image. The Hessian matrix at the point $(p, q)$ is expressed as

$$H(p, \nabla) = \begin{bmatrix} C_{pp}(G, \nabla) & C_{pq}(G, \nabla) \\ C_{pq}(G, \nabla) & C_{qq}(G, \nabla) \end{bmatrix} \quad (10)$$

Where $C_{pp}(G, \nabla)$, $C_{pq}(G, \nabla)$, and $C_{qq}(G, \nabla)$ are the convolution obtained on the second-order Gaussian derivative, and $\nabla$ is the scale factor. Let $E_{pp}, E_{qq}$, and $E_{pq}$ represents the second-order Gaussian derivative approximation, then the Hessian determinant is given as

$$det(H_{approx}) = E_{qq}E_{pp} - (\alpha E_{pq})^2 \qquad (11)$$

Where $\alpha$ represents the weight chosen as 0.9. The second-order derivative in $C_{pp}, C_{qq}$ and $C_{pq}$ are depicted in Fig 2.To maintain uniformity in feature extraction $T$ number of feature points are detected such that the feature points are represented as

$$(\hat{x}_t, \hat{y}_t) = \{(\hat{x}_1, \hat{y}_1), (\hat{x}_2, \hat{y}_2) \ldots \ldots (\hat{x}_T, \hat{y}_T)$$

**(a) TVT Feature extraction**

Once the feature points $(\hat{x}_t, \hat{y}_t)$are detected by the SURF feature extraction algorithm, the TVT transform [26] is used to extract the features along with the $3 \times 3$ neighborhood. Fig 3(a) represent the neighborhood representation of pixels around $(\hat{x}_t, \hat{y}_t)$. Let the pixel around the $3 \times 3$ neighborhood is expressed as

$$P(\hat{x}_t, \hat{y}_t) =$$
$$\begin{bmatrix} p(\hat{x}_t - 1, \hat{y}_t - 1) & p(\hat{x}_t - 1, \hat{y}_t) & p(\hat{x}_t - 1, \hat{y}_t + 1) \\ p(\hat{x}_t, \hat{y}_t - 1) & p(\hat{x}_t, \hat{y}_t) & p(\hat{x}_t, \hat{y}_t + 1) \\ p(\hat{x}_t + 1, \hat{y}_t - 1) & p(\hat{x}_t + 1, \hat{y}_t) & p(\hat{x}_t + 1, \hat{y}_t + 1) \end{bmatrix}$$
$$(12)$$

Let $P_1, P_4, P_5 P_2, P_3$denotes the center pixel,bottom right, bottom left top left, and top right pixel respectively. This can be mathematically expressed as $P_1 = p(\hat{x}_t, \hat{y}_t)$, $P_2 = p(\hat{x}_t - 1, \hat{y}_t - 1)$ , $P_3 = p(\hat{x}_t - 1, \hat{y}_t + 1)$ , $P_4 = p(\hat{x}_t + 1, \hat{y}_t + 1)$ and $P_5 = p(\hat{x}_t + 1, \hat{y}_t + 1)$ . Two triangular sections are constructed using the pixels $P_1, P_2, P_3, P_4$, and $P_5$, where the first triangular section is constructed using the pixels $P_1, P_2$ and $P_3$ as depicted in Fig 3(b), while the second triangular section is constructed using the pixels $P_4, P_5$ and $P_6$ as indicated in Fig 3(c).The TVT coefficient vertices for the pixels $P_1, P_2$ and $P_3$can be estimated using the relations

_____

$$x_1 = \left| \frac{P_2{}^2 - P_3{}^2 + P_1{}^2}{2P_1} \right| \quad (13)$$

$$y_1 = \left| \sqrt{P_2{}^2 - \frac{P_2{}^2 - P_3{}^2 + P_1{}^2}{2P_1}} \right| \quad (14)$$
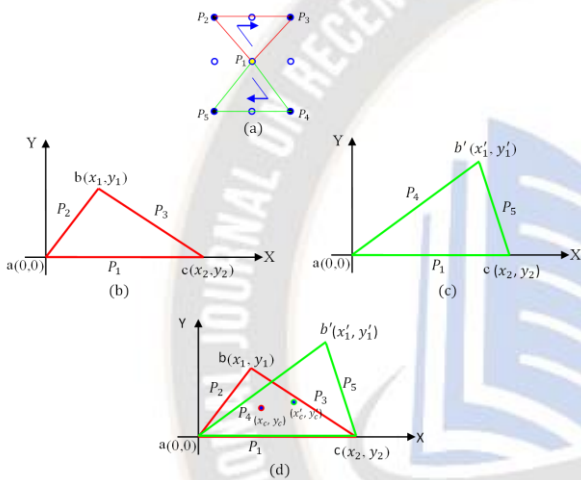
Similarly, the TVT coefficient vertices for the pixels $P_1$, $P_4$ and $P_5$ can be estimated using the relations

$$x_1' = \left| \frac{P_4{}^2 - P_5{}^2 + P_1{}^2}{2P_1} \right| \quad (15)$$

$$y_1' = \left| \sqrt{P_4{}^2 - \frac{P_4{}^2 - P_5{}^2 + P_1{}^2}{2P_1}} \right| \quad (16)$$

$$x_2 = P_1, y_2 = 0 \quad (17)$$

Therefore the vertices coefficients for the first triangular section are $a(0,0), b(x_1, y_1)$ and $c(P_1, 0)$, where the vertices coefficients for the second triangular section are $a(0,0), b(x_1', y_1')$ and $c(P_1, 0)$.



**Fig3**: Extraction of TVT features (a) Formation of the neighbourhood (b) Construction of TVT layout with pixels $P_1$, $P_2$ and $P_3$ (c) Construction of TVT

layout with pixels $P_1$, $P_4$ and $P_5$ (d) Distance estimation from the centroids

The centroid of the first triangular section is constructed from the vertices $a(0,0), b(x_1, y_1)$ and $c(x_2, y_2)$, where the centroid of the second triangular section is constructed from the vertices $a(0,0), b'(x_1', y_1')$ and $c(x_2, y_2)$. The centroid of the two triangular sections can be estimated as

$$(x_c, y_c) = \left( \frac{x_1 + P_1}{3}, \frac{y_1}{3} \right) \quad (18)$$

$$(x_c', y_c') = \left( \frac{x_1' + P_1}{3}, \frac{y_1'}{3} \right) \quad (19)$$

Thecentroid distance is expressed as

$$d = \sqrt{(x_c - x_c')^2 + (y_c - y_c')^2} \quad (20)$$

Therefore the TVT features extracted from the $l^{th}$ image is given by $d_{l,t}$ where $t = 1,2 \ldots \ldots T$. The features extracted from $L$ number of training images is

$$F_{train} = [d_{l,t}] = [d_{1,t}, d_{2,t}, d_{3,t} \ldots \ldots d_{L,t}] \quad where \; l = 1,2, \ldots \ldots L \quad (21)$$

### 2.4 Decision tree classifier

The TVT based distance features extracted from the training images $F_{train}$ are trained using the decision tree classifier.The essential patterns are estimated during the training process of the decision tree classifier. A tree-based approach is followed in the decision tree classifier for estimating the required patterns. A test on the data attribute is done while splitting the branches on the tree. The node data tuples correspond to data of one class, such that the splitting is repeated until the final level is attained. Generation of tree and pruning of the tree are the two phases in decision tree classifier. The tree along with the branches are constructed during the tree generation process, while the outliers namely branches or sub-tree are minimized during the pruning process. During the pruning process, the size of the tree is highly reduced that uses the c4.5 algorithm for Splitting.In the classification phase, the feature extracted from the test image $F_{test} = [d_{test,t}]$ is applied to the trained model to detect the classified result namely fetal abdomen, fetal femur, fetal thorax, fetal brain, maternal cervix, or other categories.

### 3. EXPERIMENTAL RESULTS

The proposed ultrasound Doppler scan image classification was validated using the parameters namely precision, specificity, F1score, accuracy, and sensitivity. We have used the publicly available ultrasound Doppler scan image dataset [28]that was scanned from $1,792$ patients, which totally has $12,400$ images. The precision, specificity, F1score, accuracy, and sensitivity are calculated using the relation shown below.

$$Precision = \frac{True_{pos}}{(True_{pos} + False_{pos})} \quad (22)$$

$$Specificity = \frac{True_{neg}}{(True_{neg} + False_{pos})} \quad (23)$$

$$F1\ Score = \frac{2 \times (precision \times sensitivity)}{precision + sensitivity} \quad (24)$$

$$Accuracy = \frac{True_{pos} + True_{neg}}{(True_{pos} + True_{neg} + False_{pos} + False_{neg})} \quad (25)$$

$$Sensitivity = \frac{True_{pos}}{(True_{pos} + False_{neg})} \quad (26)$$

Where $True_{pos}$, $False_{neg}$, $True_{neg}$, and $False_{pos}$ are the true positive, false negative, true negative, and false positive of the classification results respectively.In order to train the decision tree classifier, we have used 70%(7129 images) of

_____

the Doppler scan images and for evaluating the algorithm we have used the remaining 30% (5271 images) images. Fig 4 depicts some of the sample images used for evaluation from the ultrasound Doppler scan image classification. The decision tree classifier classifies the ultrasound scan images into six class's namely fetal thorax, fetal abdomen, fetal brain, fetal femur, maternal cervix, and other categories.



**Fig 4:** Sample test images from the dataset (a) Fetal thorax (b) Fetal abdomen (c) Fetal brain (d) Fetal femur (e) Maternal cervix (f) Others

_____



(a)          (b)          (c)          (d)
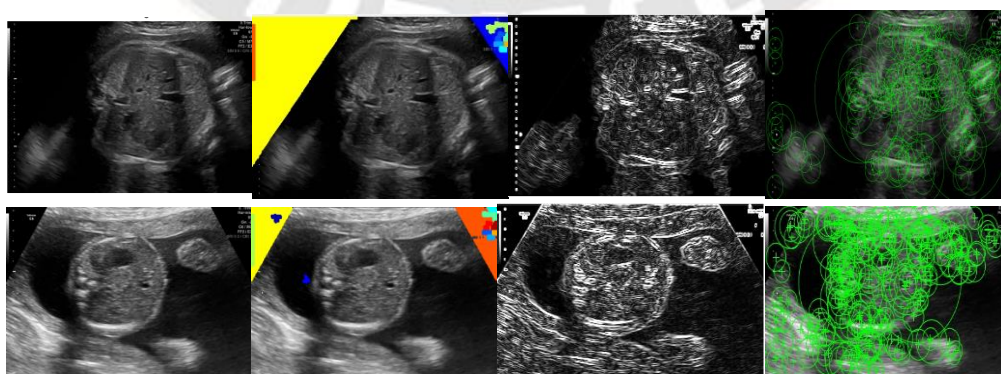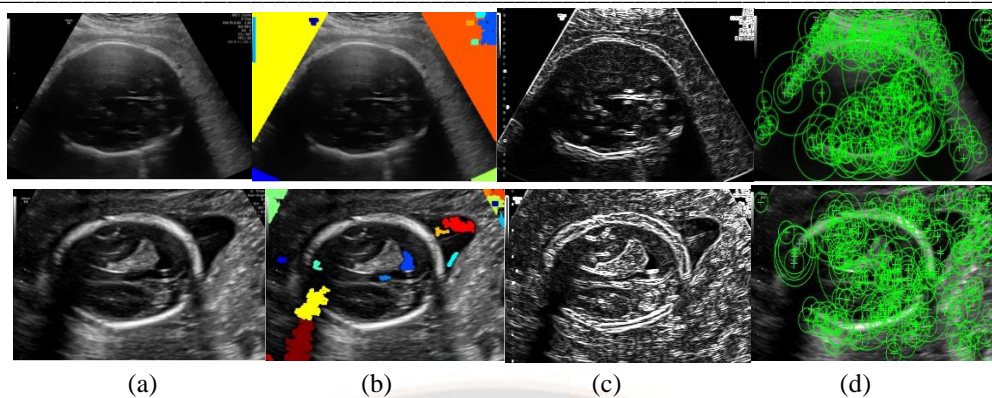
**Fig 5**: Results for the ultrasound scan image type fetal abdomen and fetal brain (row 1 and 2): fetal abdomen (row 3 and 4) fetal brain (a) Input scan image (b) MSER regions (c) Gradient Magnitude (d) SURF feature points

Fig 5 depicts the experimental results obtained for different categories of the image such as the fetal abdomen and fetal brain categories. Fig 5(a) depicts the input Doppler scan image Fig 5(b) depicts the different MSER regions obtained by the MSER algorithm. The MSER algorithm mostly eliminates the background region, where the region of interest is mostly present in the residual image. However few regions that are selected by the MSER algorithm are also selected to estimate the actual region of interest. Fig 5(c) depicts the gradient estimated on the estimated region of interest. The gradient will highlight the essential information present in the Doppler scan images. Fig 5(d) depicts the SURF feature points selected where the TVT features are extracted from the neighborhood of the SURF feature points.



(a)          (b)          (c)          (d)
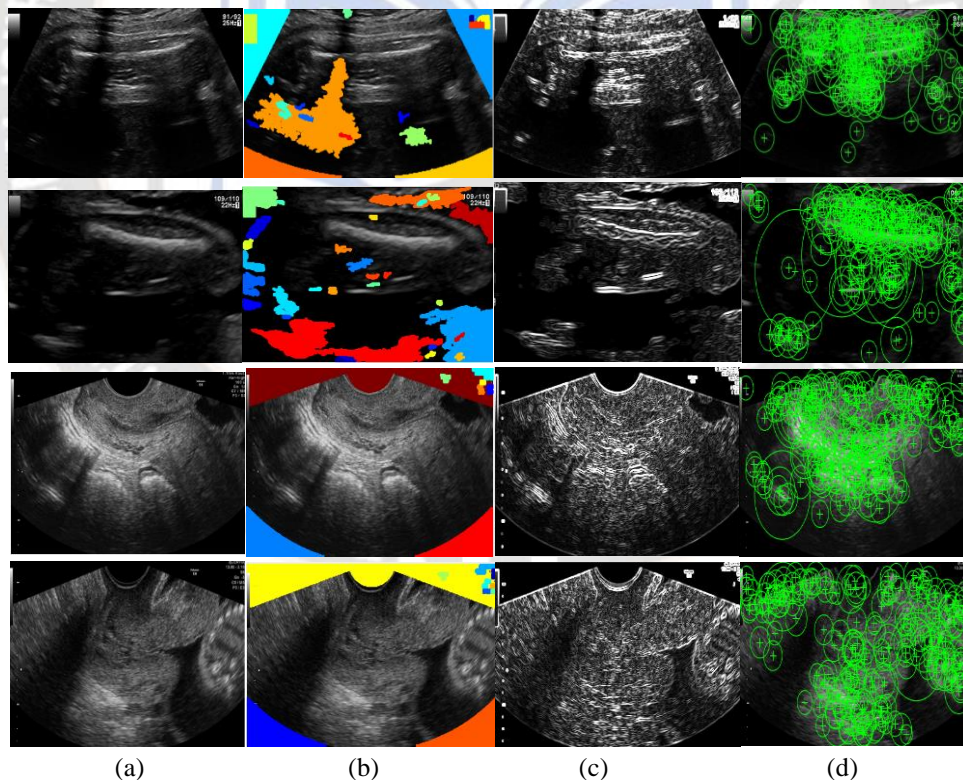
**Fig 6**: Results for the ultrasound scan image type fetal femurand maternal cervix(row 1 and 2): fetal femur (row 3 and 4) maternal cervix (a) Input scan image (b) MSER regions (c) Gradient Magnitude (d) SURF feature points  Similarly,Fig 6 and 7 depict the experimental results obtained for different categories of the image such as the fetal femur, maternal cervix, fetal thorax, and other categories.

_____



(f)
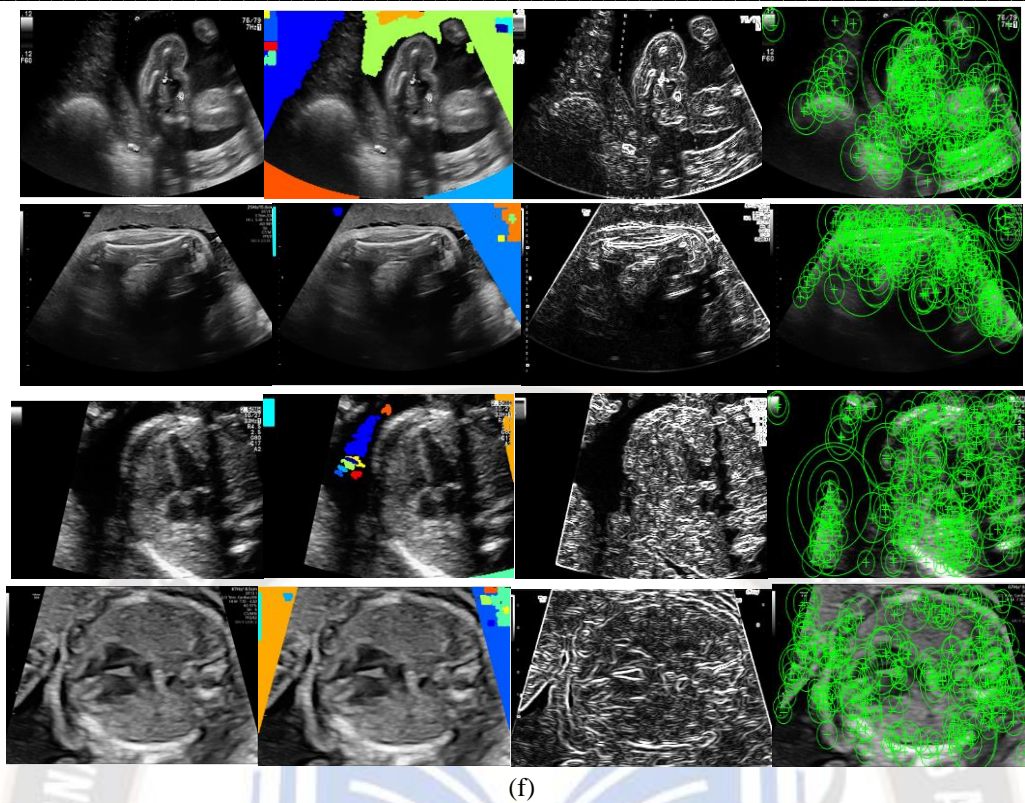
**Fig 7:**Results for the ultrasound scan image type other categoriesand fetal thorax(row 1 and 2): other categories (row 3 and 4) fetal thorax (a) Input scan image (b) MSER regions (c) Gradient Magnitude (d) SURF feature points

**Table 1:** Comparison of the proposed approach with other traditional schemes in terms of precision, specificity, F1-score, accuracy, and sensitivity

| Schemes | F1-Score (%) | Specificity (%) | Sensitivity (%) | Precision (%) | Accuracy (%) |
|---|---|---|---|---|---|
| VGG | 90.16 | 92.48 | 89.16 | 88.64 | 92.1 $\pm$ 6.1 |
| MobileNet | 90.87 | 92.01 | 90.45 | 89.07 | 87.5 $\pm$ 9.6 |
| Inception-v3 | 93.28 | 93.69 | 91.11 | 90.47 | 93.5 $\pm$ 5.0 |
| ResNet-152 | 93.71 | 95.05 | 90.32 | 91.99 | 92.8 $\pm$ 5.5 |
| ResneXt-101 | 91.73 | 94.21 | 92.89 | 90.56 | 94.0 $\pm$ 4.8 |
| SE-ResNeXt-101 | 91.89 | 96.11 | 93.01 | 92.23 | 92.7 $\pm$ 5.8 |
| DenseNet-169 | 92.45 | 97.56 | 93.66 | 93.01 | 93.6 $\pm$ 5.1 |
| **Proposed** | 94.12 | 98.73 | 95.86 | 93.57 | 97.96$\pm$1.48 |

The traditional approach namely DenseNet-169 [29], SE-ResNeXt-101 [30], ResneXt-101 [31], ResNet-152 [32], Inception-v3 [33], MobileNet [34], VGG [35] are compared with the proposed ultrasound Doppler scan image classification system. The precision, specificity, F1-score, sensitivity and accuracy of the proposed scheme was estimated as 93.57% , 98.73% , 94.12% , 95.86% and 97.96% respectively. The proposed method has improvement in accuracy of3.967% and 4.36%than the the ResneXt-101 and DenseNet-169 respectively. The precision of the proposed method is 0.56% and 1.34%more than the DenseNet-169 and SE-ResNeXt-101 scheme respectively. The sensitivity, specificity and F1-Sore of the proposed method is 2.2%, 1.17%, 1.67% higher than the DenseNet-169 approach respectively.
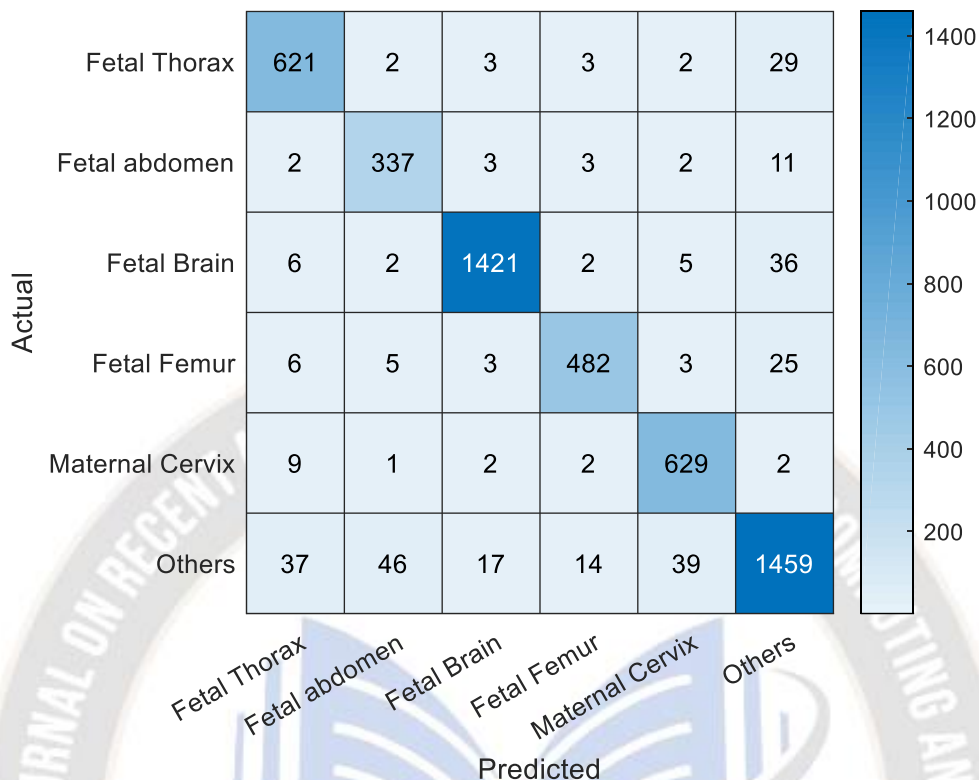
83

_____



**Fig 8:** Confusion matrix obtained on the test image classification
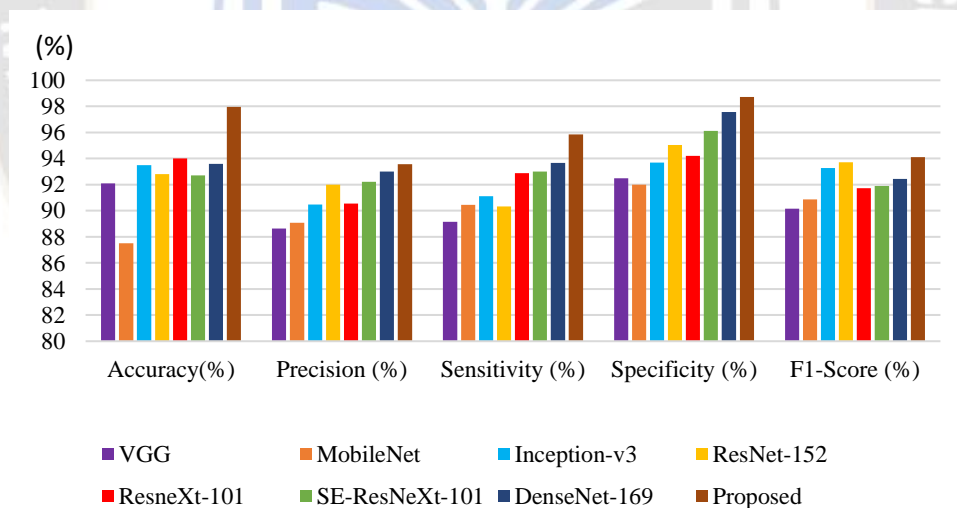


**Fig 9:** Graphical comparison of different classifiers with the proposed classification system

The confusion matrix obtained during the testing is depicted in Fig 8. The graphical comparison of sensitivity, accuracy, specificity, precision, and F1-score of the proposed approach is depicted in Fig 9. The comparison shows that the proposed approach provides a good performance than the traditional methods.

_____

**Table 2**: Comparison of time complexity and accuracy for different number of feature points $T$

| T | Accuracy (%) | Time of training (s) | Time of classification (s) |
|---|---|---|---|
| 50 | 87.14 | 3,053 | 0.53 |
| 100 | 91.27 | 3,827 | 0.62 |
| 150 | 94.18 | 4,432 | 0.79 |
| 200 | 96.8 | 5,101 | 0.89 |
| 250 | 97.33 | 5,933 | 0.99 |
| **300** | *97.96* | *6,453* | *1.13* |
| 350 | 97.63 | 6,981 | 1.28 |
| 400 | 97.28 | 5,436 | 1.37 |

Table II depicts the accuracy and time complexity comparison for different values of $T$. The experiment was evaluated for a different number of SURF feature points $T$. As the number of feature points increases from $50$, the accuracy increases from $87.14\%$. The accuracy reaches a maximum of $97.96\%$ when the number of feature points is chosen as $T = 300$. For further increase of feature points, the accuracy gets reduced from $97.96\%$. For the number of feature points $T = 300$, the training time is estimated as $6,453$ seconds. With $T = 300$, the time of classification is estimated as $1.13$ seconds.

**Table 3:** Comparison of the proposed method with and without using region selection

| Method | Accuracy (%) | Time of training (s) | Time of classification (s) |
|---|---|---|---|
| With region selection | *97.96* | 6,453 | 1.13 |
| Without region selection | 94.21 | *5,821* | *0.97* |

Table III depicts the comparison of the proposed approach without the use of region selection and using the region selection. Without using the region selection process, the proposed approach provides an accuracy of 94.21%, while using the region selection process the accuracy increases by 3.75%. However, the time of training and classification will be reduced without using the region selection process.
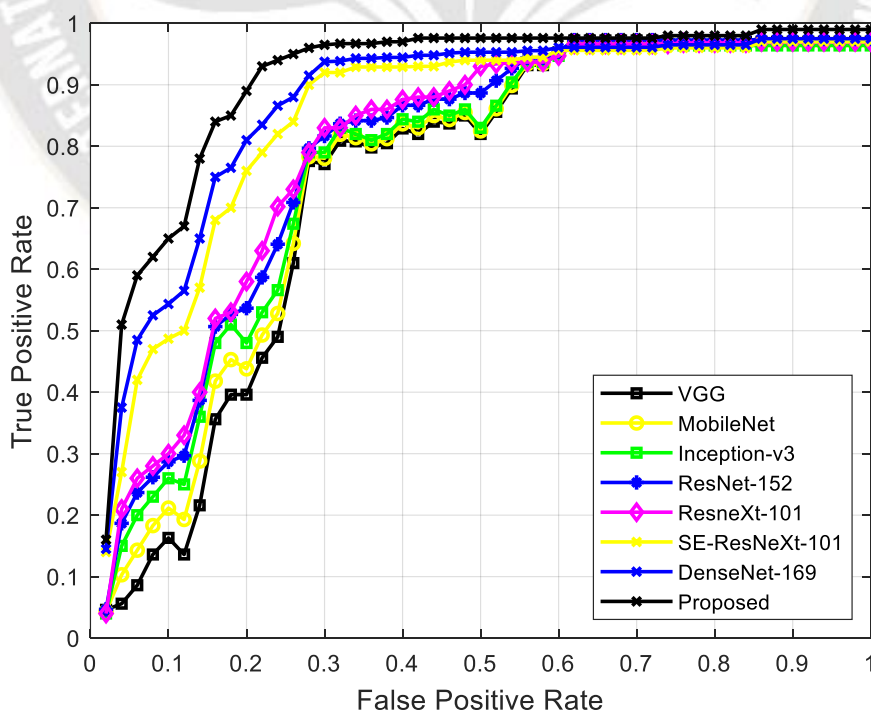


**Fig 10**: ROC curve comparison of the proposed method with other traditional approaches

**85**

_____

The ROC comparison of traditional approaches like Inception-v3, MobileNet, VGG, SE-ResNeXt-101, ResneXt-101, ResNet-152, and DenseNet-169 with the proposed Doppler scan image classification system is shown in Fig 10. The proposed scheme provides an AUC of 0.9286 which is higher than the traditional method.

## 4. CONCLUSION

This paper proposed the Doppler ultrasound scan image classification algorithm that uses the residual of maximally stable external regions and the decision tree classifier. The algorithm initially pre-processes the image and estimates the maximally stable regions using the MSER algorithm. From the estimated MSER regions, a few regions are selected that best describe the ROI along with the residual region. SURF Feature points are then detected in the resulting ROI after the estimation of the gradient. The neighborhood around the SURF feature points is used to estimate the TVT feature. The extracted features are then trained/classified using the decision tree classifier to classify the scan images as the fetal femur, fetal thorax, fetal abdomen, fetal brain, maternal cervix, and other categories. The experimental evaluation was done using the big data ultrasound scan image datasetwith the metrics such as F1 score, sensitivity, accuracy, specificity, and precision. The proposed approach provides an F1-score, specificity, precision, sensitivity, and accuracy of 94.12%, 98.73%, 93.57%, 95.86%, and 97.96% respectively. Evaluation results reveal that the proposed algorithm outperforms the traditional ultrasound scan image classification algorithms.

## REFERENCES

[1]. Ben Yedder, Hanene, Ben Cardoen, and Ghassan Hamarneh. "Deep learning for biomedical image reconstruction: a survey." *Artificial Intelligence Review* 54.1 (2021): 215-251.

[2]. Dalal, Navneet, and Bill Triggs. "Histograms of oriented gradients for human detection." *2005 IEEE computer society conference on computer vision and pattern recognition (CVPR'05)*. Vol. 1. Ieee, 2005.

[3]. Chaudhary, D. S. . (2022). Analysis of Concept of Big Data Process, Strategies, Adoption and Implementation. International Journal on Future Revolution in Computer Science &Amp; Communication Engineering, 8(1), 05–08. https://doi.org/10.17762/ijfrcsce.v8i1.2065

[4]. Firdous, & Mir, M. (2016). Intellectual Property Rights Issues and Challenges of Academic Libraries in Digital Environment. *International Journal of Computer Engineering in Research Trends*, *3(12)*, 2349–7084

[5]. Murthuja, P. (2019.). *Big data in healthcare: Challenges and approaches", International Journal of Computer Engineering In Research Trends, 6(5):pp 317-321, May 2019.*.

[6]. Tzotsos, Angelos, and Demetre Argialas. "Support vector machine classification for object-based image analysis." *Object-Based Image Analysis*. Springer, Berlin, Heidelberg, 2008. 663-677.

[7]. Lai, ZhiFei, and HuiFang Deng. "Medical image classification based on deep features extracted by deep model and statistic feature fusion with multilayer perceptron." *Computational intelligence and neuroscience* 2018 (2018).

[8]. Arora, Siddharth, et al. "Multilevel thresholding for image segmentation through a fast statistical recursive algorithm." *Pattern Recognition Letters* 29.2 (2008): 119-125.

[9]. Chudasama, Diya, et al. "Image segmentation using morphological operations." *International Journal of Computer Applications* 117.18 (2015).

[10]. Litjens, G. *et al*. A survey on deep learning in medical image analysis. *Med. image analysis* 42, 60–88 (2017).

[11]. Suchetha, M., Rajiv Raman, and Edwin Dhas. "Region of Interest based Predictive Algorithm for Subretinal Hemorrhage Detection using Faster R-CNN." (2021).

[12]. Chandrakar, I. (2022). Improved Technique for Preserving Privacy while Mining Real Time Big Data. International Journal of Communication Networks and Information Security (IJCNIS), 14(1).

[13]. Esteva, A. *et al*. Dermatologist-level classification of skin cancer with deep neural networks. *Nat.* 542, 115 (2017).

[14]. Das, Sraddha, et al. "Deep learning architecture based on segmented fundus image features for classification of diabetic retinopathy." Biomedical Signal Processing and Control 68 (2021): 102600.

[15]. Hosny, A., Parmar, C., Quackenbush, J., Schwartz, L. H. & Aerts, H. J. Artificial intelligence in radiology. *Nat. Rev. Cancer* **18**, 500 (2018).

[16]. Lee, Lok Hin, Yuan Gao, and J. Alison Noble. "Principled Ultrasound Data Augmentation for Classification of Standard Planes." International Conference on Information Processing in Medical Imaging. Springer, Cham, 2021.

[17]. Attallah, Omneya, Maha A. Sharkas, and Heba Gadelkarim. "Fetal brain abnormality classification from MRI images of different gestational age." Brain sciences 9.9 (2019): 231.

[18]. Sridar, Pradeeba, et al. "Decision fusion-based fetal ultrasound image plane classification using convolutional neural networks." Ultrasound in medicine & biology 45.5 (2019): 1259-1273.

[19]. Xie, H. N., et al. "Using deeplearning algorithms to classify fetal brain ultrasound images as normal or abnormal." Ultrasound in Obstetrics & Gynecology 56.4 (2020): 579-587.

[20]. Qiao, Sibo, et al. "RLDS: An explainable residual learning diagnosis system for fetal congenital heart disease." Future Generation Computer Systems 128 (2022): 205-218.

_____

[21]. Sushma, T. V., et al. "Classification of Fetal Heart Ultrasound Images for the Detection of CHD." Innovative Data Communication Technologies and Application. Springer, Singapore, 2021. 489-505.

[22]. Maraci, M., Bridge, C., Napolitano, R., Papageorghiou, A. & Noble, J. A framework for analysis of linear ultrasound videos to detect fetal presentation and heartbeat. Med. *Image Analysis* **37**, 22–36 (2017).

*[23].* Ryou, H. *et al*. Automated 3d ultrasound biometry planes extraction for first trimester fetal assessment. In *Machine Learning in Medical Imaging*, 196–204 (2016).

[24]. Li, Y. *et al*. Standard plane detection in 3d fetal ultrasound using an iterative transformation network. *Medical Image Computing and Computer Assisted Intervention – MICCAI* **2018**, 392–400 (2018).

[25]. Donoser, Michael, and Horst Bischof. "Efficient maximally stable extremal region (MSER) tracking." *2006 IEEE computer society conference on computer vision and pattern recognition (CVPR'06)*. Vol. 1. Ieee, 2006.

[26]. Tang, Jiali, et al. "Image edge detection based on singular value feature vector and gradient operator." *Mathematical Biosciences and Engineering* 17.4 (2020): 3721-3735.

[27]. Joy, P., Thanka, R., & Edwin, B. (2022). Smart Self-Pollination for Future Agricultural-A Computational Structure for Micro Air Vehicles with Man-Made and Artificial Intelligence. International Journal of Intelligent Systems and Applications in Engineering, 10(2), 170–174. Retrieved from https://ijisae.org/index.php/IJISAE/article/view/1743

[28]. Bay, Herbert, et al. "Speeded-up robust features (SURF)." *Computer vision and image understanding* 110.3 (2008): 346-359.

[29]. Prabha, K., and I. Shatheesh Sam. "A novel blind color image watermarking based on Walsh Hadamard Transform." *Multimedia Tools and Applications* 79.9 (2020): 6845-6869.

[30]. Polat, Kemal, and Salih Güneş. "A novel hybrid intelligent method based on C4. 5 decision tree classifier and one-against-all approach for multi-class classification problems." *Expert Systems with Applications* 36.2 (2009): 1587-1592.

[31]. Burgos-Artizzu, Xavier P., et al. "Evaluation of deep convolutional neural networks for automatic classification of common maternal fetal ultrasound planes." *Scientific Reports* 10.1 (2020): 1-12.

[32]. Burgos-Artizzu, Xavier P., et al. "Evaluation of deep convolutional neural networks for automatic classification of common maternal fetal ultrasound planes." *Scientific Reports* 10.1 (2020): 1-12.

[33]. Hu, J., Shen, L. & Sun, G. Squeeze-and-excitation networks. CoRR abs/1709.01507 (2017).

*[34].* Xie, S., Girshick, R., Dollar, P., Tu, Z. & He, K. Aggregated residual transformations for deep neural networks. In *Proceedings of the IEEE Conference on Computer Vision and Pattern Recognition*, 1492–1500 (2017).

*[35].* *André Sanches Fonseca Sobrinho. (2020). An Embedded Systems Remote Course. Journal of Online Engineering Education, 11(2), 01–07. Retrieved from http://onlineengineeringeducation.com/index.php/joee/article/view/39*

[36]. He, K., Zhang, X., Ren, S. & Sun, J. Deep residual learning for image recognition. CoRR abs/1512.03385 (2015).

[37]. Szegedy, C. *et al*. Going deeper with convolutions. CoRR abs/1409.4842 (2014).

*[38].* Sandler, M., Howard, A., Zhu, M., Zhmoginov, A. & Chen, L.-C. Mobilenetv2: Inverted residuals and linear bottlenecks. *CVPR*(2018).

[39]. Simonyan, K. & Zisserman, A. Very deep convolutional networks for large-scale image recognition. CoRR abs/1409.1556 (2014).